Journal of Power Sources 189 (2009) 59–65

Contents lists available at ScienceDirect

Journal of Power Sources

journal homepage: www.elsevier.com/locate/jpowsour

Effect of firing temperature on the electrochemical performance of $LiMn_{0.4}Fe_{0.6}PO_4$/C materials prepared by mechanical activation

Dong-Ho Baek[a], Jae-Kwang Kim[a], Yong-Jo Shin[a], Ghanshyam S. Chauhan[a], Jou-Hyeon Ahn[a,*], Ki-Won Kim[b]

[a] Department of Chemical and Biological Engineering and Engineering Research Institute, Gyeongsang National University, 900 Gajwa-dong, Jinju 660-701, Republic of Korea
[b] School of Nano and Advanced Materials Engineering and Engineering Research Institute, Gyeongsang National University, 900 Gajwa-dong, Jinju 660-701, Republic of Korea

ARTICLE INFO

Article history:
Received 8 July 2008
Received in revised form 20 October 2008
Accepted 17 November 2008
Available online 21 November 2008

Keywords:
Phospho-olivine
$LiMn_yFe_{1-y}PO_4$
Mechanical activation
Synthetic variables
Electrochemical performance

ABSTRACT

Carbon-coated $LiMn_{0.4}Fe_{0.6}PO_4$ composites ($LiMn_{0.4}Fe_{0.6}PO_4$/C) were synthesized for use as cathode materials in lithium batteries. The composites were synthesized by a mechanical activation process that consists of high-energy ball milling for 10 h, followed by thermal treatment at different temperatures. The structure, particle size and surface morphology of these cathode active materials were investigated by inductively coupled plasma (ICP) analysis, energy dispersive spectrometry (EDS), high-resolution Raman spectroscopy, X-ray diffraction (XRD), field emission scanning electron microscopy (FE-SEM), and high-resolution transmission electron microscopy (HR-TEM). The firing temperature was observed to affect morphology, particle size, elemental distribution, structure of the residual carbon, and consequently the electrochemical properties of the composites. $LiMn_{0.4}Fe_{0.6}PO_4$/C synthesized at 600 °C possessed the most desirable properties and it exhibited the best performance when used as cathode in lithium batteries at room temperature. The cell, comprising cathode of this composite, exhibited the initial discharge capacities of 144.5 mAh g^{-1} (85.0% of theoretical capacity) and 122.0 mAh g^{-1} (71.8%), respectively, at 0.1 and 1 C-rates. The cathode showed good cycle stability without substantial capacity fade up to 50 cycles.

1. Introduction

In recent years, the olivine phosphates with chemical formula $LiMPO_4$ (where M denotes Fe, Mn, Co, Ni) have attracted the attention of battery technologists who are looking to develop efficient positive electrode materials for use in lithium batteries. However, these materials have poor electronic conductivity in comparison to $LiCoO_2$ (10^{-3} S m^{-1}), which is currently used as cathode material. Hence, there have been attempts to enhance the electronic conductivity of $LiMPO_4$ by designing new synthetic strategies and by optimizing synthetic conditions. The frequently reported methods include *in situ* carbon coating on particles and doping of metal ions that coexist with Li^+ in $LiMPO_4$. The synthesis of $LiMPO_4$ has been reported by sol–gel method [1–3]. The energy density, capacity delivery and life cycle of $LiMPO_4$ have been enhanced by the dispersion of low concentration of metal ions (Cu or Ag) in the sol precursor [4]. The coating of carbon on $LiMPO_4$ particles by using organic additives enhances their electrochemical performance [5]. A wide range of carbon precursors offers flexibility to this method. The synthesis of $LiMPO_4$ can be accomplished in multiple steps or in a single step by firing it at high temperature [6]. However, this method involves complex procedures and takes a long time [7].

Out of all the olivine phosphates, $LiMnPO_4$ should have been the desirable candidate for use as positive cathode material. The Mn^{3+}/Mn^{2+} redox couple in the olivine framework is positioned at 4.1 V versus Li/Li^+ which is reasonably high, compared to 3.4 V of Fe^{3+}/Fe^{2+} redox couple in $LiFePO_4$. However, Mn^{3+}/Mn^{2+} redox couple has some serious drawbacks that limit its use as cathode material. $LiMnPO_4$ has much lower current durability and much smaller effective energy density than $LiFePO_4$. It also exhibits comparatively slower kinetics [8]. The major reason for its poor electrochemical activity is the large kinetic barrier at the mismatched interface of $MnPO_4/LiMnPO_4$ [9]. To utilize its inherent high capacity, some attempts have been made to synthesize mixed olivine phosphates with a general formula of $LiMn_yFe_{1-y}PO_4$ where the amounts of Mn can be manipulated in a desirable proportion. The manipulation of y in $LiMn_yFe_{1-y}PO_4$ can be used to optimize its properties to tailor a promising candidate material that has an operating cell voltage of 3.4–4.1 V versus Li^+/Li. The desirable amount of Mn in the $LiMn_yFe_{1-y}PO_4$ composition is crucial, as cathode material with higher Mn amount has poorer cycling stability. Ma and Qin synthesized $LiMn_yFe_{1-y}PO_4$ thin films by using modified elec-

* Corresponding author. Tel.: +82 55 751 5388; fax: +82 55 753 1806.
E-mail address: jhahn@gnu.ac.kr (J.-H. Ahn).

0378-7753/$ – see front matter © 2008 Elsevier B.V. All rights reserved.
doi:10.1016/j.jpowsour.2008.11.051

trostatic spray deposition and sol–gel technique [10]. The results showed that the electrode made of thin film of $LiMn_{0.4}Fe_{0.6}PO_4$ exhibited better electrochemical performance than that of pure $LiFePO_4$ and $LiMnPO_4$. The synthesis of $LiMn_yFe_{1-y}PO_4$ by solid state reactions has been reported [11,12]. The conventional solid state method is often followed, since it usually results in high purity of the material if the raw materials are blended thoroughly to achieve homogeneity. However, the processing steps are lengthy and most often complex, requiring repeated steps of grinding, heating, pelletizing and firing at high temperature [13,14]. These steps result in large micron-sized particles. The solid state mechanical activation (MA) method has been recently found to be efficient in synthesizing sub-micron-sized cathode active materials [15–18]. In this process, the ingredients are thoroughly mixed together initially in a high-energy ball mill. The milling process helps to reduce time and temperature of the subsequent firing steps, and hence it is advantageous to prevent the undesirable growth of crystals which usually occurs at higher temperature. We have earlier reported synthesis of $LiFePO_4$, carbon-coated $LiFePO_4$ and $LiMPO_4$ following MA process [15,16]. It was observed that process parameters such as ball milling time and firing temperature significantly influence $LiFePO_4$ properties [15]. A direct coating of carbon over the active material particles is achieved by adding acetylene black powder as the carbon source. In this article, we report a parametric study for the influence of firing temperature on the structure and properties of carbon-coated $LiMn_{0.4}Fe_{0.6}PO_4$/C. The electrochemical properties of these composites were studied. The composite synthesized at 600 °C exhibited the best performance. The variation in the firing temperature affected the particle size and morphology of the composites. $LiMn_{0.4}Fe_{0.6}PO_4$/C(600) exhibited good cycle performance when used as cathode in lithium batteries at room temperature. It exhibited the initial discharge capacities of 144.5 mAh g^{-1} and 122.0 mAh g^{-1}, respectively, at 0.1 C and 1 C current densities, and no capacity fade was observed up to 50 cycles.

2. Experimental

2.1. Synthesis of $LiMn_{0.4}Fe_{0.6}PO_4$/C

$LiMn_{0.4}Fe_{0.6}PO_4$/C composites were synthesized from Li_2CO_3, $FeC_2O_4{\cdot}2H_2O$, $Mn(COOCH_3)_2{\cdot}4H_2O$ and $NH_4H_2PO_4$ (all chemicals of 99% purity from Aldrich) taken in stoichiometric quantities [15]. For carbon coating, acetylene black (Alfa, purity >99.9%) was added in proportion of 7.8 wt.% of the total weight. The mechanical activation process consisted of the following steps: high-energy ball milling of the powder in a hardened steel vial with zirconia balls (ball-to-powder weight ratio = 10:3) at room temperature for different periods in an argon atmosphere using a SPEX mill at 1000 rpm; conversion of the powder into pellets by mechanical pressing; thermal treatment of the pellets at temperatures ranging from 500 °C to 800 °C for 10 h in a nitrogen atmosphere, respectively. For the sake of simplicity and to highlight the firing temperature, the samples were designated as $LiMn_{0.4}Fe_{0.6}PO_4$/C(500), $LiMn_{0.4}Fe_{0.6}PO_4$/C(600), $LiMn_{0.4}Fe_{0.6}PO_4$/C(700), and $LiMn_{0.4}Fe_{0.6}PO_4$/C(800).

2.2. Characterization of synthesized materials

The crystallographic structure of the synthesized materials was analyzed by X-ray powder diffraction (XRD) (D8 Advance, Bruker AXS) using Cu Kα radiation (3 kW). Scanning electron microscopy (SEM) imaging was carried by using field-emission scanning microscopy (FE-SEM) (Philips XL30 S FEG). The nature and thickness of carbon coating were observed with high-resolution transmission electron microscopy (HR-TEM) (JEM-2010, JEOL). The elemental distribution in the composites was confirmed with energy dispersive X-ray spectrometry. The chemical composition of the composites was determined by inductively coupled plasma (ICP) analysis (Atomscan 25, Optima 4300DV) and carbon content by elemental analyzer (CHNS-932, LECO). To understand the structure of the carbon, high-resolution Raman spectra were recorded on LabRAM HR800 UV.

2.3. Electrochemical evaluation

To prepare the cathode, $LiMn_{0.4}Fe_{0.6}PO_4$/C powder, Super-P carbon black (Alfa) and poly(vinylidene fluoride) (PVdF, Aldrich) binder were mixed in 80:10:10 weight ratio in N-methylpyrrolidone (NMP) to make a viscous slurry that was cast on aluminum foil and dried at 95 °C under vacuum for 12 h. The film was cut into circular discs of area 0.785 cm^2 and mass ~2.0 mg for use as cathode.

The coin type Li/$LiMn_{0.4}Fe_{0.6}PO_4$ cell was fabricated by stacking lithium metal (300 μm thickness, Cyprus Foote Mineral Co.) anode and $LiMn_{0.4}Fe_{0.6}PO_4$-based cathode with Celgard® 2200 separator film. 1 M $LiPF_6$ in ethylene carbonate (EC)/dimethyl carbonate (DMC) (Samsung Cheil Industries Inc.) (1:1 by volume) was used as liquid electrolyte. The cell assembly was performed under argon atmosphere in a glove box (H_2O < 10 ppm). Cyclic voltammetry (CV) was done at a scan rate 0.1 mV s^{-1} between 2.0 V and 4.6 V vs. Li/Li^+. The charge–discharge and cycling properties of Li/$LiMn_{0.4}Fe_{0.6}PO_4$ cells were evaluated between 2.0 V and 4.6 V at 0.1 C (0.03 mA cm^{-2}) and 1 C (0.3 mA cm^{-2}) current densities using an automatic galvanostatic charge–discharge unit (WonA Tech. Co.) at room temperature.

3. Results and discussion

The structural, morphological and electrochemical properties of $LiMn_{0.4}Fe_{0.6}PO_4$/C composites have been studied. The mechanical activation process is a superior option to obtain a material with good electrochemical performance [19]. The composites were prepared by ball milling for 15 h, and that was then followed by heating for 10 h at different temperatures (500 °C, 600 °C, 700 °C or 800 °C). The chemical composition of the samples obtained from ICP analysis matched the theoretical molar ratio of Li:Mn:Fe:P as 1.00:0.40:0.60:1.00 and all the composites contain 13.6 wt.% carbons, which was obtained from elemental analysis and was controlled by using the optimized synthetic conditions to have the same carbon content in the composites. The XRD spectra of the composites matched the standard $LiFePO_4$ as shown in Fig. 1. The

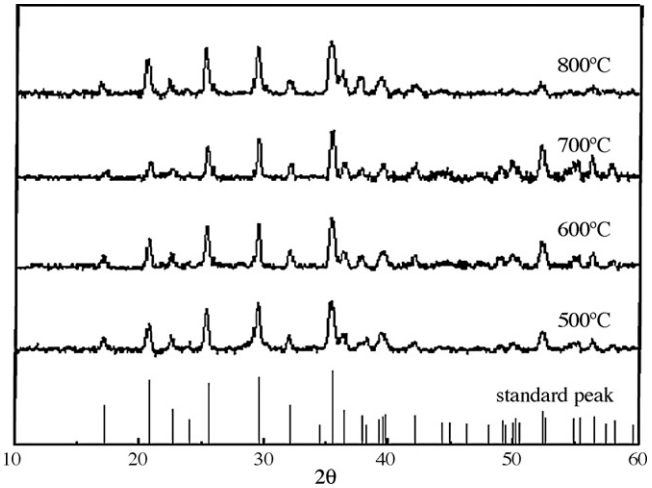

Fig. 1. XRD spectra of $LiMn_{0.4}Fe_{0.6}PO_4$/C composites synthesized at different firing temperatures.

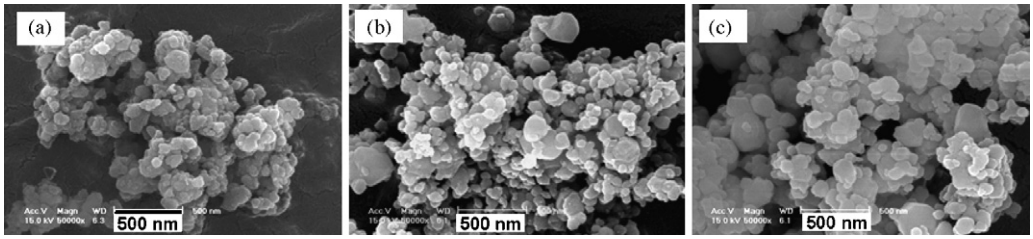

Fig. 2. SEM pictures of (a) $LiMn_{0.4}Fe_{0.6}PO_4$/C(600), (b) $LiMn_{0.4}Fe_{0.6}PO_4$/C(700), and (c) $LiMn_{0.4}Fe_{0.6}PO_4$/C(800).

crystalline nature of the composites is depicted from the spectra. The composites have crystalline structures belonging to the orthorhombic *Pnma* group. These have sharp crystalline peaks in the 2θ region from 20 to 40, as noticeable differences can be observed beyond $2\theta = 40$. The sharpest peaks can be observed for $LiMn_{0.4}Fe_{0.6}PO_4$/C(600), meaning thereby that high crystallization was achieved at 600 °C. We have already reported an attainment of a reasonable extent of crystallinity in $LiFePO_4$ by firing at 500 °C

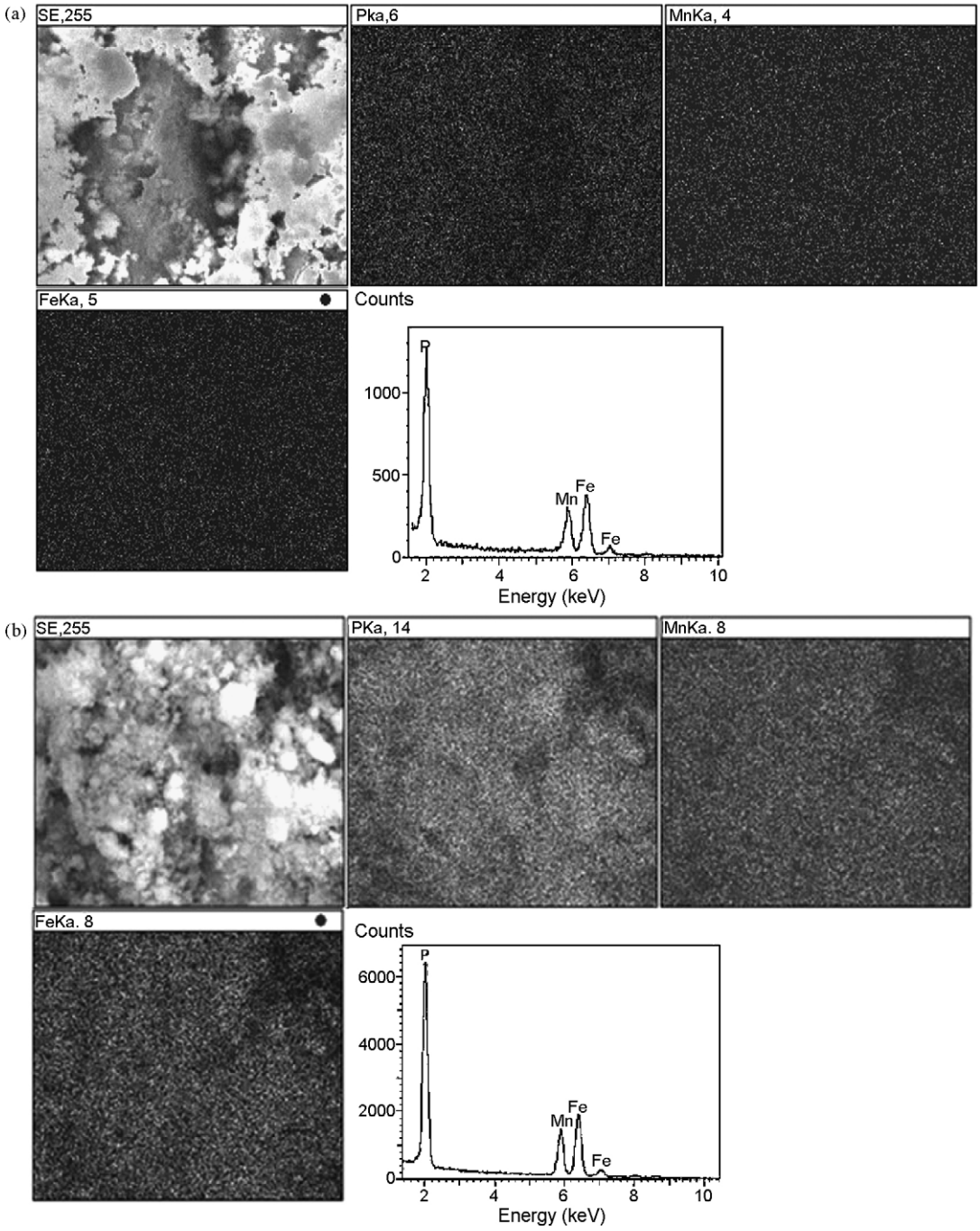

Fig. 3. SEM pictures and the corresponding EDS maps of P, Mn and Fe of (a) $LiMn_{0.4}Fe_{0.6}PO_4$/C(600) and (b) $LiMn_{0.4}Fe_{0.6}PO_4$/C(700) composites.

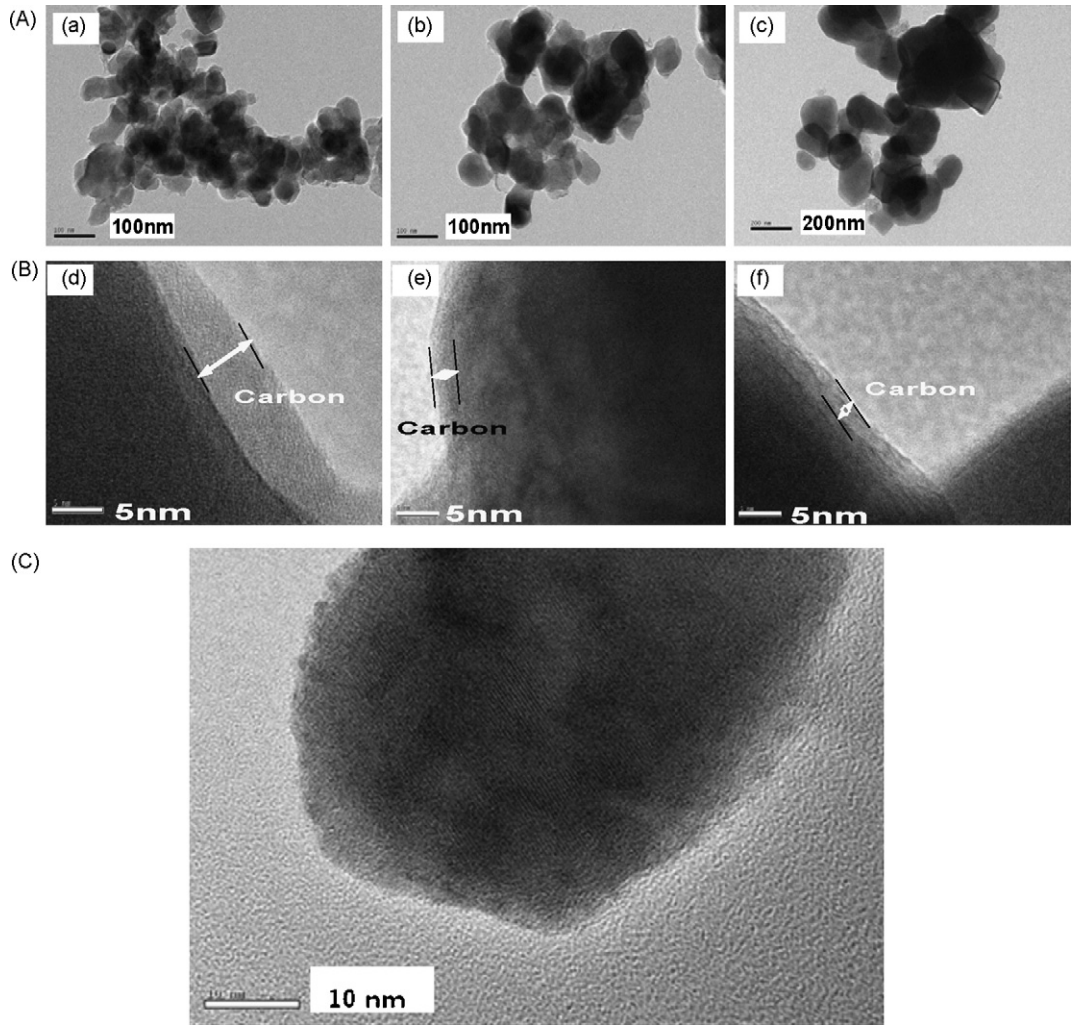

Fig. 4. (A) TEMs of (a) $LiMn_{0.4}Fe_{0.6}PO_4$/C(600), (b) $LiMn_{0.4}Fe_{0.6}PO_4$/C(700), and (c) $LiMn_{0.4}Fe_{0.6}PO_4$/C(800) composites. (B) Carbon coating thickness in (d) $LiMn_{0.4}Fe_{0.6}PO_4$/C(600), (e) $LiMn_{0.4}Fe_{0.6}PO_4$/C(700), and (f) $LiMn_{0.4}Fe_{0.6}PO_4$/C(800) composites. (C) TEM image (10 nm scale) of $LiMn_{0.4}Fe_{0.6}PO_4$/C(600) composite.

[15]. The absence of Fe_2P or other parasitic peaks was confirmed from the XRD analysis. The presence of carbon source during synthesis ensures impurities-free particles, where the oxidation of Fe^{2+} is checked and any Fe^{3+} is reduced back to Fe^{2+} [20]. The carbon coating limits the size of the particles and improves the electrochemical performance of the active material by enhancing electrical conductivity. It also affects reversible capacity of the material [21].

The heat treatment in the mechanical activation process has a marked influence on the morphological properties of the samples. Fig. 2 shows SEM images of three $LiMn_{0.4}Fe_{0.6}PO_4$/C samples. The particle size of the composites was found to vary from ~50 nm to ~200 nm with more particles on the lower side

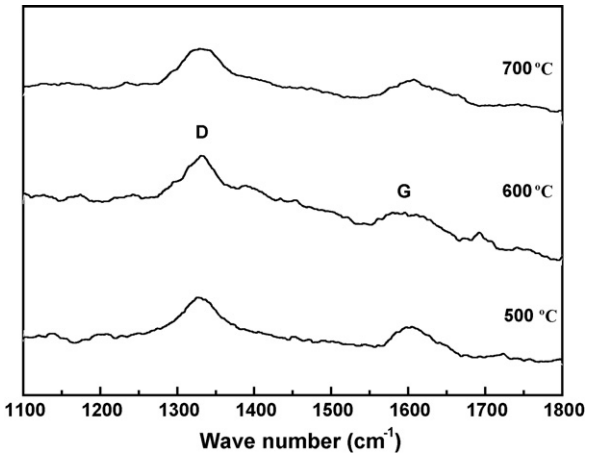

Fig. 5. HR-Raman spectra of $LiMn_{0.4}Fe_{0.6}PO_4$/C composites prepared at different temperatures.

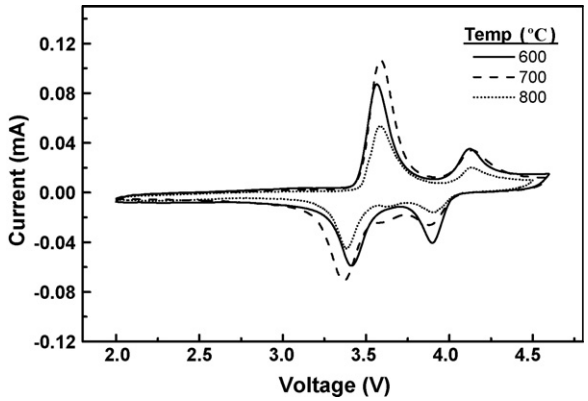

Fig. 6. First CV curves of different $LiMn_{0.4}Fe_{0.6}PO_4$/C composites (scan rate: 0.1 mV s^{-1}, voltage range: 2.0–4.6 V).

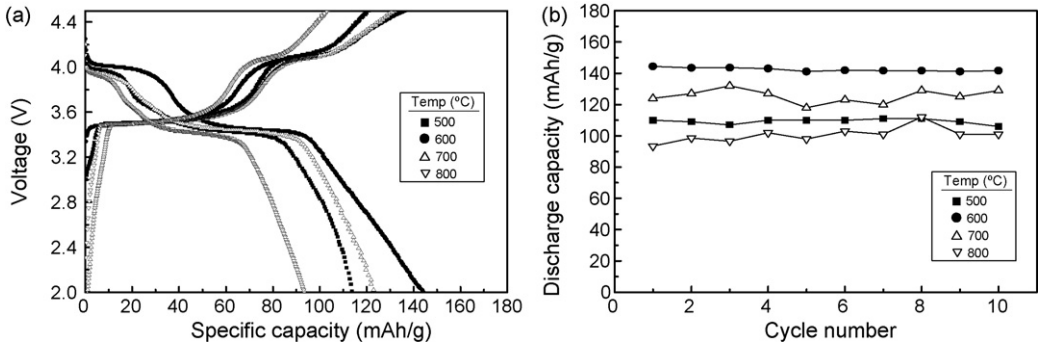

Fig. 7. (a) Initial charge–discharge curve and (b) cycle behavior of $LiMn_{0.4}Fe_{0.6}PO_4$/C composites.

of this spectrum. The particle size homogeneity is more visible in $LiMn_{0.4}Fe_{0.6}PO_4$/C(600) than in the other two samples. Though the carbon coating resulted in small nano-sized particles, yet the agglomeration of particles with an increase of synthetic temperature is evident as can be seen from the SEM of $LiMn_{0.4}Fe_{0.6}PO_4$/C(800) [22]. The homogeneous distribution of P, Mn and Fe in $LiMn_{0.4}Fe_{0.6}PO_4$/C(600) can be observed from the SEM and the corresponding EDS analysis of the sample [Fig. 3(a)]. The same is not true for $LiMn_{0.4}Fe_{0.6}PO_4$/C(700) as the uneven elemental distribution as shown in Fig. 3(b). The chemical composition by the EDS analysis was again confirmed to match the theoretical molar ratio of Mn:Fe:P for both the composites.

TEM images of all the $LiMn_{0.4}Fe_{0.6}PO_4$/C composites are shown in Fig. 4. The average particle size was 60 nm, 80 nm, and 200 nm for the composites synthesized at 600 °C, 700 °C, and 800 °C, respectively. The effect of the synthetic temperature on the particle size is evident as at higher temperatures the agglomeration of particles resulted in the particles of bigger size as can be observed from the TEM of $LiMn_{0.4}Fe_{0.6}PO_4$/C(800). $LiMn_{0.4}Fe_{0.6}PO_4$/C(600) has the smallest particles with a narrow particle size distribution. The nature and extent of the carbon coating are important factors which affect the electrochemical properties of olivine phosphates. A uniform carbon coating of ~10 nm is enough to make an effective contribution to the electronic conductivity of olivine phosphates [23]. A nanometer-sized web of the amorphous carbon (that appears as waves in light shade) surrounding the $LiMn_{0.4}Fe_{0.6}PO_4$ particles (those appear as the dark regions) can be seen in the TEM images [Fig. 4(b)]. TEM image of $LiMn_{0.4}Fe_{0.6}PO_4$/C(600) at 10 nm scale is shown in Fig. 4(c). $LiMn_{0.4}Fe_{0.6}PO_4$ crystallite appears in a straight line form with dark regions, and the carbon coating of the composite appears in a wave form with greyish regions [24].

The coating of amorphous carbon with a thickness of 4–8 nm was observed as nano-web in all the samples. A thin conductive matrix along with small particle size positively affects the electronic conductivity of the composites. The structure of the carbon coating was determined from HR-Raman spectra. The perusal of Fig. 5 reveals that the D(disordered)/G(graphene) ratios in $LiMn_{0.4}Fe_{0.6}PO_4$/C(600) and $LiMn_{0.4}Fe_{0.6}PO_4$/C(700) are nearly the same at 1.03 and 1.15, respectively. The disordered carbon is sp^3-coordinated carbon, and graphene is a single planar sheet of sp^2-bonded carbon [25]. Hence, lower D/G ratio, more conductive is the coated carbon. Even a small difference in the D/G ratio can result in different electrochemical properties of these composites [26].

The electrochemical properties of these materials were evaluated as cathode materials for lithium batteries at room temperature. Two sets of oxidation and reduction peaks typical for Mn^{3+}/Mn^{2+} and Fe^{3+}/Fe^{2+} in $LiMn_{0.4}Fe_{0.6}PO_4$ composites are present in the CV curves obtained for the first cycle as shown in Fig. 6. The single redox peak pair for Fe^{3+}/Fe^{2+} redox couple exhibited an anodic oxidation potential at 3.55 V, 3.6 V, and 3.59 V and a cathodic reduction potential at 3.4 V, 3.35 V, and 3.38 V with a respective peak separation of 150 mV, 250 mV, and 250 mV between the anodic and cathodic peaks, respectively, for $LiMn_{0.4}Fe_{0.6}PO_4$/C(600), $LiMn_{0.4}Fe_{0.6}PO_4$/C(700), and $LiMn_{0.4}Fe_{0.6}PO_4$/C(800). The redox current difference of 0.061 mA, 0.073 mA, and 0.045 mA has been observed for $LiMn_{0.4}Fe_{0.6}PO_4$/C(600), $LiMn_{0.4}Fe_{0.6}PO_4$/C(700), and $LiMn_{0.4}Fe_{0.6}PO_4$/C(800), respectively. For Mn^{3+}/Mn^{2+}, the corresponding values for the anodic and cathodic peaks are at 4.1 V and 3.9 V for all the samples, and a redox current difference of 0.045 mA, 0.027 mA, and 0.02 mA for $LiMn_{0.4}Fe_{0.6}PO_4$/C(600), $LiMn_{0.4}Fe_{0.6}PO_4$/C(700), and $LiMn_{0.4}Fe_{0.6}PO_4$/C(800), respectively. On account of the differences in redox current in the redox couples, $LiMn_{0.4}Fe_{0.6}PO_4$/C(600) and $LiMn_{0.4}Fe_{0.6}PO_4$/C(700) showed higher application potential compared to $LiMn_{0.4}Fe_{0.6}PO_4$/C(800). $LiMn_{0.4}Fe_{0.6}PO_4$/C(600) showed the highest redox current in Mn^{3+}/Mn^{2+} redox reaction. For both the redox couple, the oxidation and reduction peaks were the sharpest in $LiMn_{0.4}Fe_{0.6}PO_4$/C(600). It indicated efficient charge-transfer kinetics for this material. It resulted from the fine crystalline structure, purity, the smallest particle size, and thin carbon coating.

$LiMn_{0.4}Fe_{0.6}PO_4$/C(600) performed better than the other composites as it delivered higher charge and discharge capacities when tested under the same current density, 0.1 C (0.03 $mAcm^{-2}$), as shown in Fig. 7(a). The initial discharge capacities obtained were 113.8 mAh g^{-1}, 144.5 mAh g^{-1}, 124.0 mAh g^{-1} and 93.4 mAh g^{-1}, respectively, for $LiMn_{0.4}Fe_{0.6}PO_4$/C(500), $LiMn_{0.4}Fe_{0.6}PO_4$/C(600), $LiMn_{0.4}Fe_{0.6}PO_4$/C(700) and $LiMn_{0.4}Fe_{0.6}PO_4$/C(800). $LiMn_{0.4}Fe_{0.6}PO_4$/C(600) exhibited better performance with a high active material utilization of ~85% during discharge. It also showed an

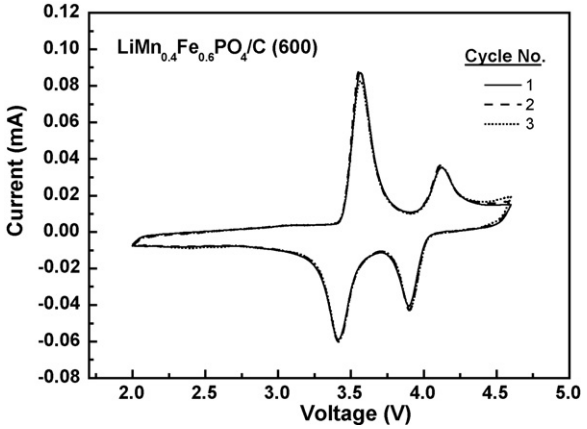

Fig. 8. CV curves of $LiMn_{0.4}Fe_{0.6}PO_4$/C(600) during cycling (scan rate: 0.1 mV s^{-1}, voltage range: 2.0–4.6 V).

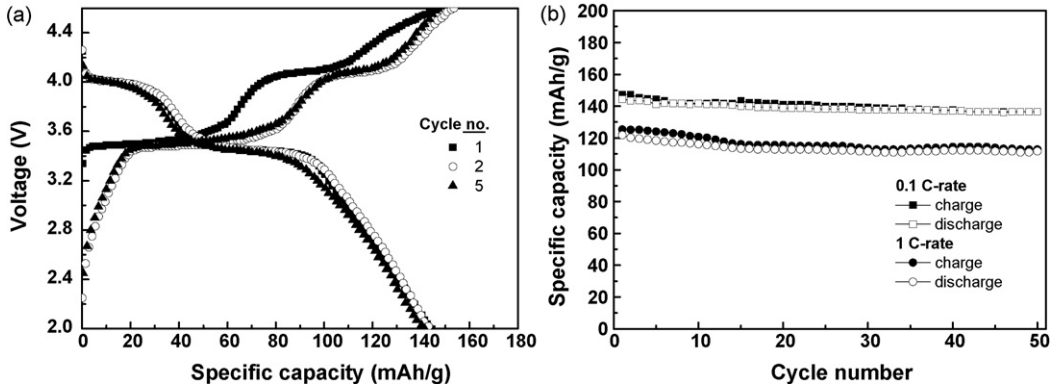

Fig. 9. (a) Specific charge–discharge capacities in cycles 1, 2, 5 and (b) cycle performance of $LiMn_{0.4}Fe_{0.6}PO_4$/C(600) composite.

almost stable performance up to 10 cycles with a minor decrease from 144.5 mAh g^{-1} to 141.7 mAh g^{-1}. In other three cases, the discharge capacities were lower than those were observed for $LiMn_{0.4}Fe_{0.6}PO_4$/C(600). The $LiMn_{0.4}Fe_{0.6}PO_4$/C(700) showed cyclical variation with an increase of cycle numbers. Given that the carbon contents of the composites were the same, the difference in the D/G ratios, the nature of carbon coating, and the particle size are likely to be the factor that contributed to the better performance of $LiMn_{0.4}Fe_{0.6}PO_4$/C(600) than the other composites [27].

From the CV behavior of $LiMn_{0.4}Fe_{0.6}PO_4$/C(600) it was observed that after three cycles, the anodic and cathodic peak positions of the redox couples did not change, as is apparent from the comparison of CV during the first, second and third cycles of the cell prepared with cathodes made of $LiMn_{0.4}Fe_{0.6}PO_4$/C(600) as shown in Fig. 8. The performance during the first cycle was retained during the subsequent cycles also. A good cycle stability and high reversibility of the redox reaction were attained on cycling for this cell. Efficient redox reaction kinetics was observed at a low discharge current. The charge–discharge performance of the lithium cell prepared with $LiMn_{0.4}Fe_{0.6}PO_4$/C(600) is shown in Fig. 9(a). The charge capacity in the range of 154–144 mAh g^{-1} and discharge capacity in the range of 144.5–141.7 mAh g^{-1} were obtained after cycles 1, 2 and 5. The cathode made with $LiMn_{0.4}Fe_{0.6}PO_4$/C(600) showed cycle stability as almost flat curves for the charge and discharge were obtained up to 50 cycles. The charge and discharge capacities became stable after 5 cycles. A reasonably good value for both charge and discharge capacities was observed at 136.6 mAh g^{-1} after 50 cycles at 0.1 C-rate, with a negligible capacity fade of ~0.15 mAh g^{-1} per cycle and a high material utilization of 80.4% [Fig. 10 (b)]. At 1 C-rate, the initial discharge capacity obtained was 122 mAh g^{-1}, and the corresponding value was 111 mAh g^{-1} after 50 cycles. After 50 cycles, with a small capacity fade of ~0.22 mAh g^{-1} per cycle, a high material utilization of 65.3% was achieved. The small particle size and amorphous carbon coating contributed to the good cycle stability and electrochemical properties of the composite, making it a promising cathode material capable of delivering satisfactory performance at room temperature.

4. Conclusions

Four carbon-coated olivine phosphates having a formula of $LiMn_{0.4}Fe_{0.6}PO_4$/C were synthesized by the variation of firing temperature, which affected their particle size and surface morphology. With the increase of the firing temperature, the particle size increased from nanometers to large micron-sized agglomerates, especially at 800 °C. The carbon nanocoating appeared as a nano-web of 4–8 nm thickness on the particles. $LiMn_{0.4}Fe_{0.6}PO_4$/C synthesized at 600 °C had the smallest particles with a narrow particle size distribution. The anodic and cathodic peaks for the Mn^{3+}/Mn^{2+} and Fe^{3+}/Fe^{2+} redox couples were ascertained from the CV curves of the composites and these indicated efficient reversibility of redox kinetics. The optimum electrochemical performance was exhibited by $LiMn_{0.4}Fe_{0.6}PO_4$/C synthesized at 600 °C with initial discharge capacities of 144.5 mAh g^{-1} and 122 mAh g^{-1} at 0.1 and 1 C-rates, respectively. The cells prepared with this sample also showed the stable cycle performance and material utilization of 80.4% as 65.3%, respectively, at 0.1 and 1 C-rates after 50 cycles.

Acknowledgements

This research was supported by the Ministry of Knowledge Economy, Korea, under the Information Technology Research Center (ITRC) support program supervised by the Institute of Information Technology Assessment (IITA). Ghanshyam S. Chauhan gratefully acknowledges the Brain Pool Fellowship.

References

[1] M.M. Doeff, Y.O. Hu, F. McLarnon, R. Kostecki, Eletrochem. Solid-State Lett. 6 (2002) A207.
[2] J.B. Lu, Z.T. Zhang, Z.L. Tang, W.C. Shen, Y.X. Xu, Rare Metal Mater. Eng. 32 (2003) 499.
[3] K.F. Hsu, S.Y. Tsay, B.J. Hwang, J. Mater. Chem. 14 (2004) 2690.
[4] F. Croce, A.D. Epifanio, J. Hassoun, A. Deptula, T. Olczac, B. Scrosati, Eletrochem. Solid-State Lett. 5 (2002) A47.
[5] Y. Hu, M.M. Doeff, R. Kostecki, R. Finones, J. Electrochem. Soc. 151 (2004) A1279.
[6] C. Delacourt, P. Poizot, M. Morcrette, J.M. Tarascon, C. Masquelier, Chem. Mater. 16 (2004) 93.
[7] A. Yamada, M. Hosoya, S.C. Chung, Y. Kudo, K. Hinokuma, K.Y. Liu, Y. Nishi, J. Power Sources 119–121 (2003) 232.
[8] G. Li, H. Azuma, M. Tohda, Electrochem. Solid-State Lett. 5 (2002) A135.
[9] C. Delacourt, L. Laffont, R. Bouchet, C. Wurm, J.B. Leriche, M. Morcrette, J.M. Tarascon, C. Masquelier, J. Electrochem. Soc. 152 (2005) A913.
[10] J. Ma, Q.Z. Qin, J. Power Sources 148 (2005) 66.
[11] T. Nakamura, K. Sakumoto, S. Seki, Y. Kobayashi, M. Tabuchi, Y. Yamada, J. Electrochem. Soc. 154 (2007) A1118.
[12] A. Yamada, Y. Takei, H. Koizumi, N. Sonoyama, R. Kanno, K. Itoh, M. Yonemura, T. Kamiyama, Chem. Mater. 18 (2006) 804.
[13] H.S. Kim, B.W. Cho, W.I. Cho, J. Power Sources 132 (2004) 235.
[14] A. Yamada, S.C. Chung, K. Hinokuma, J. Electrochem. Soc. 148 (2001) A224.
[15] J.K. Kim, G. Cheruvally, J.W. Choi, J.U. Kim, J.H. Ahn, G.B. Cho, K.W. Kim, H.J. Ahn, J. Power Sources 166 (2007) 211.
[16] Y.J. Shin, J.K. Kim, G. Cheruvally, J.H. Ahn, K.W. Kim, J. Phys. Chem. Solids 69 (2008) 1253.
[17] S.J. Kwon, C.W. Kim, W.T. Jeong, K.S. Lee, J. Power Sources 137 (2004) 93.
[18] X.Z. Liao, Z.F. Ma, L. Wang, X.M. Zhang, Y. Jiang, Y.S. He, Electrochem. Solid-State Lett. 7 (2004) A522.
[19] S. Franger, F.L. Cras, C. Bourbon, H. Rouault, J. Power Sources 119–121 (2003) 252.
[20] Y.H. Rho, L.F. Nazar, L. Perry, D. Ryan, J. Electrochem. Soc. 154 (2007) A283.
[21] R. Dominko, M. Bele, M. Gaberscek, M. Remskar, D. Hanzel, S. Pejovnik, J. Jamnik, J. Electrochem. Soc. 152 (2005) A607.
[22] C.H. Mi, X.B. Zhao, G.S. Cao, J.P. Tu, J. Electrochem. Soc. 152 (2005) A483.

[23] H. Gabrisch, J.D. Wilcox, M.M. Doeff, Electrochem. Solid-State Lett. 9 (2006) A360.
[24] G.T.K. Fey, T.L. Lu, J. Power Sources 178 (2008) 807.
[25] A.K. Geim, K.S. Novoselov, Nat. Mater. 6 (2007) 183.
[26] J.K. Kim, J.W. Choi, G.S. Chauhan, J.H. Ahn, G.C. Hwang, J.B. Choi, H.J. Ahn, Electrochim. Acta 53 (2008) 8258.
[27] C. Delacourt, P. Poizot, S. Levasseur, C. Masquelier, Electrochem. Solid-State Lett. 9 (2006) A350.